RSC Advances

PAPER

View Article Online
View Journal | View Issue

Cite this: *RSC Adv.*, 2021, **11**, 9469

Porous graphene nanocages with wrinkled surfaces enhancing electrocatalytic activity of lithium/sulfuryl chloride batteries

Xiangyang Li,[ab] Hirbod Maleki Kheimeh Sari,[c] Lanjie Niu,*[b] Gege He,[a] Yao Zhou,[d] Xifei Li*[c] and Zhanbo Sun*[a]

The lithium/sulfuryl chloride battery has been used as a primary power source because of its high energy/power density and level of safety. However, disadvantages regarding the sluggish kinetics of the electrode materials have limited its further energy related applications. Herein, we report an efficient approach to prepare nitrogen-doped graphene nanocages with high surface roughness to overcome this issue. The combination of a porous wrinkled surface and hollow structure can properly accommodate the volume-change, promote charge transfer, and enhance structural stability. The designed composite electrode can deliver an initial voltage as high as 3.58 V, an advanced discharge time of 840 s, and an outstanding relative capacity (63.20 mA h) and rate capability (29.36%). This unique structure engineering strategy also provides a potentially cost-effective way for synthesizing other carbon materials and their application in various electrochemical energy storage devices.

Received 23rd December 2020
Accepted 23rd February 2021

DOI: 10.1039/d0ra10756e

rsc.li/rsc-advances

1. Introduction

The lithium/sulfuryl chloride (Li/SO_2Cl_2) battery, possessing a high energy density and specific power, wide operating temperature range, stable discharge voltage, and high level of safety, have been considered as one of the most potential reserve batteries for utilization in borehole operation, oil-gas production and orientation navigation fields.[1–4] Nonetheless, they have some drawbacks such as a large current discharge ability, voltage delay, and corrosive anode material which could greatly hinder their practical applications.[5,6] To overcome these obstacles, considerable strategies have been presented in recent years. In this regard, employing the modified anode electrode materials in Li/SO_2Cl_2 batteries is suggested as the most cost-effective approach, which could improve the discharge current and capacity along with discharge voltage to a certain extent. The design of anode material is primarily focused on the rate capability and specific capacity, while is highly dependent on the capacitive materials with an available surface area or triggering of fast redox reactions at the electrode/electrolyte interface.[7,8] Although further researches are still required about the modified anode materials, many electrode materials, including graphite, metal oxides, dichalcogenides, carbides, MXenes, and MOFs have been widely investigated as high-performance electrode materials.[9–15] Despite the significant advances achieved in this regard, the energy and power densities are much lower than expected,[2,16] and the obtained high energy density is usually at the expense of sacrificing power density.[17,18] Furthermore, with increasing power density, the energy density reveals a tendency to dramatic decrease due to the kinetics imbalance between the battery-type and capacitor-type electrodes.[19] Moreover, most of these electrode materials have other issues, such as complex synthesis procedures, being environmentally hazardous, high cost, and poor electrical conductivity and large volume-change during the lithiation/delithiation process, which result in a deteriorated rate capability and fast capacity decay, and impede their scale-up deployment.[20–24] Therefore, a compatible strategy needs to be taken into effect to develop nanostructured composites with small diffusion distance in a solid phase, and improve the performance of Li/SO_2Cl_2 batteries with superior rate capability and specific capacity along with a fast charge–discharge capability.

Herein, we demonstrate an effective approach that creates a porous wrinkled structure in N-doped graphene nanocages to address the above issues, in which 3-hydroxytyramine hydrochloride with aid of a hard template from silica micro-sphere was used as the carbon source. The as-prepared electrode material for Li/SO_2Cl_2 battery can effectively shorten the ion diffusion length, improve electron conductivity and facilitate electrolyte diffusion.

[a]*School of Physics, MOE Key Laboratory for Non-Equilibrium Synthesis and Modulation of Condensed Matter, Key Laboratory of Shaanxi for Advanced Functional Materials and Mesoscopic Physics, Xi'an Jiaotong University, Xi'an 710049, People's Republic of China. E-mail: szb@mail.xjtu.edu.cn*

[b]*Science and Technology on Electromechanical Dynamic Control Laboratory, Xi'an Institute of Electromechanical Information Technology, Xi'an 710065, People's Republic of China. E-mail: nljwl@163.com*

[c]*Institute of Advanced Electrochemical Energy, School of Materials Science and Engineering, Xi'an University of Technology, Xi'an, Shaanxi 710048, People's Republic of China. E-mail: xfli2011@hotmail.com*

[d]*School of Materials and Energy, Yunnan University, Kunming 650091, People's Republic of China*

The thickness of the graphene shell layer of N-doped graphene nanocages was calculated to be about 16 nm. The acquired graphene nanocages endowed Li/SO_2Cl_2 battery with a high initial voltage of 3.58 V, a long discharge time of 840 s, an excellent relative capacity of 63.20 mA h and a rate capability of 29.36%. This research is a novel study on the application of N-doped graphene nanocages in Li/SO_2Cl_2 battery, which can draw further attention to the development of the high performance energy storage devices.

2. Experimental section

2.1 Chemicals

Silica micro-sphere, cobaltous acetate, 3-hydroxytyramine hydrochloride and methyl alcohol were obtained from Aladdin Industrial Corporation. Hydrofluoric acid, sulfuric acid and anhydrous ethanol were purchased from Sinopharm Chemical Reagent Co., Ltd. Deionized water (18.25 MΩ cm) was used in all of the preparations. All chemicals were of analytical grade and used as-received without further purification.

2.2 Synthesis of hollow and porous carbon nanostructure

The hollow and porous carbon nanostructure was synthesized *via* a facile hydrothermal procedure. Typically, silica micro-sphere (0.7 g) was dispersed in the methyl alcohol solution (20 mL) under ultrasonic dispersion and vigorous magnetic stirring. Then, $Co(CH_3COO)_2 \cdot 4H_2O$ (0.5978 g) was rapidly injected into the mixture solvent, and 0.5689 g of 3-hydroxytyramine hydrochloride was also added into the mixture with strong stirring for 30 min. The suspension was stirred at 65 °C in a water bath to emit methyl alcohol. Afterwards, the collected mixture was calcined under nitrogen flow at 600 °C for 1 h and 800 °C for 2 h, and the silica template was etched by hydrofluoric acid and sulfuric acid. Subsequently, the hollow and porous carbon nanostructure was collected through centrifugation and washed with distilled water and ethanol for several times and dried at 80 °C for 8 h.

2.3 Characterization of the samples

The morphology of the samples was investigated with a field emission scanning electron microscope (FESEM, FEI Quanta 450) at an accelerating voltage of 15 kV, and a high resolution transmission electron microscope (TEM, JEOL JEM-2100) at an accelerating voltage of 200 kV. Powder X-ray diffraction (XRD) pattern was recorded by a Bruker-AXS D8 Advance diffractometer operated at 40 kV voltage and 30 mA current using Cu Kα radiation (λ = 1.5418 Å) in the range of 15–90°. Raman spectroscopy was measured using a Renishaw inVia Qontor Raman spectrometer with 532 nm excitation wavelength. X-ray photoelectron spectroscopy (XPS) was performed by means of a Kratos Axis UL equipped with monochromatic Al Kα radiation (150 W, 5 kV at 1486.6 eV), and the surface charge was corrected by referencing the spectra to the C 1s peak for the C–C bond at a binding energy of 284.8 eV.

2.4 Electrochemical measurements of the samples

The electrochemical testing was conducted in the simulated Li/SO_2Cl_2 batteries, and was performed by CHI 660E under an

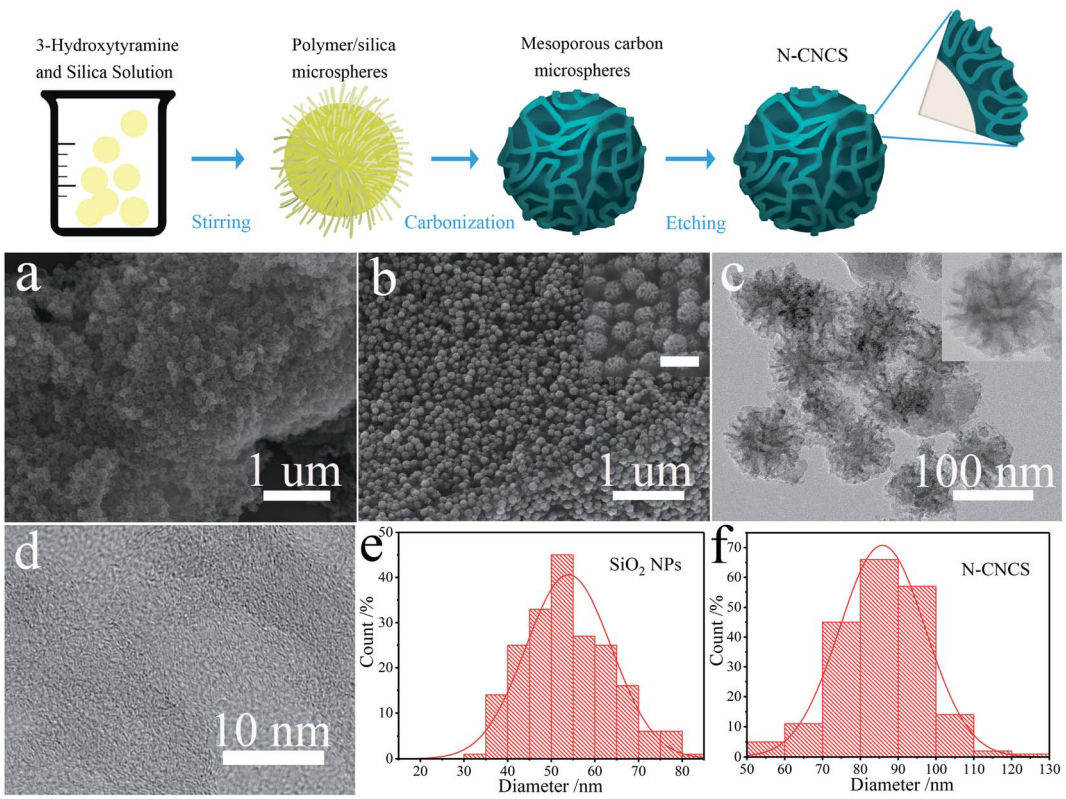

Fig. 1 Schematics of the synthesis process for N-CNCS, FESEM images of the silica (a) and N-CNCS (b), respectively, the scale bar in the inset of (b) is 100 nm. (c) TEM and (d) HRTEM images of N-CNCS. Particle size distribution for silica (e) and N-CNCS (f).

argon atmosphere at 23–25 °C. In a simulated cell, the cathode (the diameter of 14 mm) was prepared by fully blending the nitrogen-doped graphene nanocages, acetylene black, conductive agent, and Teflon emulsion, the mass ration of acetylene black (the nitrogen-doped graphene nanocages as a certain proportion): conductive agent: Teflon emulsion was 70 : 20 : 10. Then, the homogeneous slurry was rolled and dried for 24 h at 150 °C. The lithium foil was used as the anode with the same diameter as the cathode. In addition, polypropylene (the diameter of 14 mm) and $LiAlCl_4$–SO_2Cl_2 solutions (1.47 mol L^{-1}, 1 mL) were employed as the separator and electrolyte, respectively. A resistance of 40 Ω was the constant load in the test. The whole discharge process of a Li/SO_2Cl_2 battery was displayed visually through the discharge curves and finished until the discharge voltage reaches to 2 V continuously. Electrochemical impedance spectra were performed in the frequency range from 10^6 Hz to 10^{-1} Hz at an amplitude of 5 mV.

3. Results and discussion

3.1 Microstructures and characterization

Herein, the approach to synthesize the nitrogen-doped carbon nanocages with high surface roughness (N-CNCS) *via* a simple heating process is proposed (Fig. 1). FESEM and TEM were carried out for morphological and structural analysis of the obtained silica micro-sphere and N-CNCS. The particles of silica have a smooth surface and homogeneous spherical morphology with a diameter of about 53.79 nm (Fig. 1a and e). When silica micro-sphere was used as the hard template and reacted with 3-hydroxytyramine hydrochloride in methanol solution, the first synthesized step of the monodispersed N-CNCS was the polymerization of 3-hydroxytyramine hydrochloride in the presence of cobaltous acetate. Then the product was calcined under the N_2 gas flow and subsequently etched using hydrofluoric acid and sulfuric acid, resulting in the formation of the targeted hollow and porous carbon nanoshells that contain doped nitrogen atoms (Fig. 1b, N-CNCS). The monodispersed N-CNCS were further characterized by TEM and HRTEM, as shown in Fig. 1c and d. It is noteworthy that the core of silica has been etched with a strong acid solution, while the structure of the N-CNCS with a homogenous and corrugated carbon shell is evident, and the thickness of the wrinkled graphene on the surface of the porous graphene nanoshells is statistically measured to be 6.3 nm. Such combined architecture constructs a buffering matrix and forms a micro-structured network for N-CNCS nanoparticles.[18,25] Further inspection by HRTEM demonstrated a clear multi-shell graphene structure with a size of ~10 nm and porous architecture, indicating that due to the

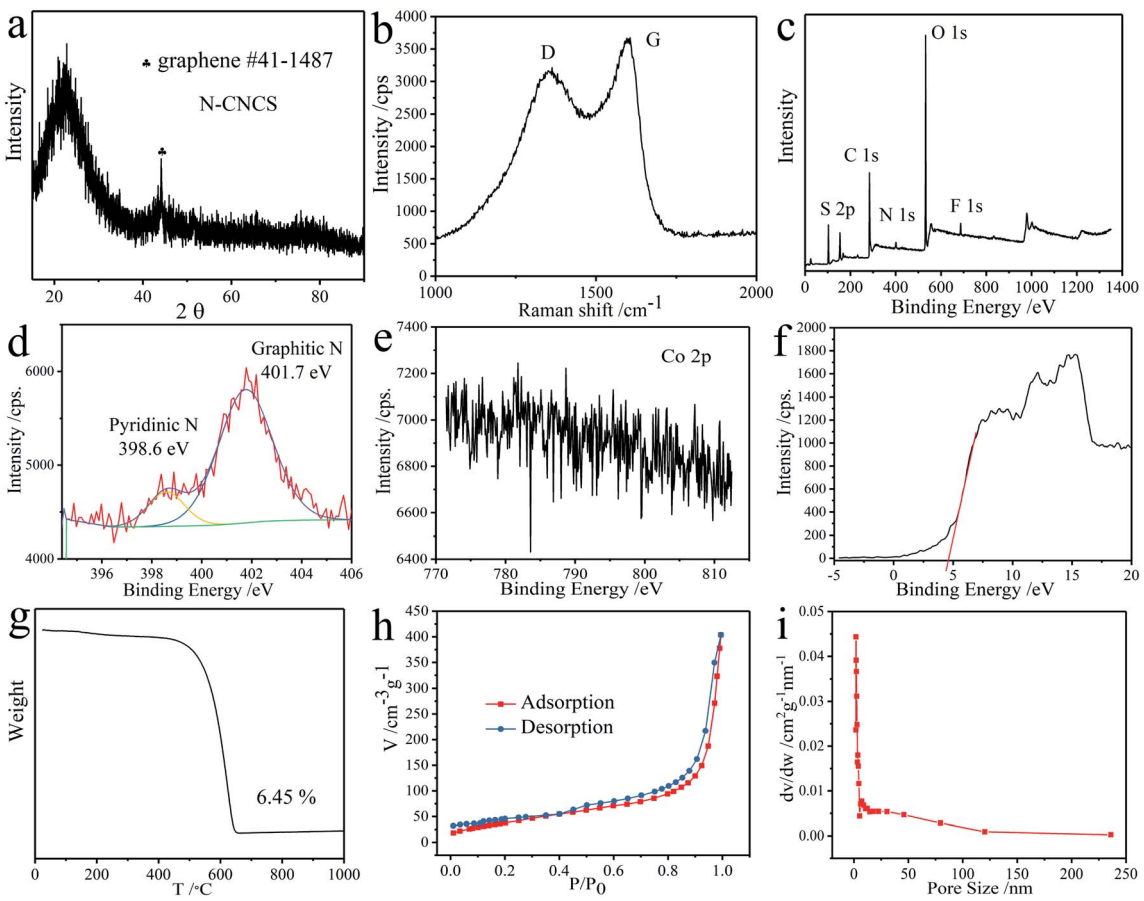

Fig. 2 (a) XRD pattern, (b) Raman spectra, (c) XPS full spectrum, (d) high-resolution N 1s XPS spectrum, (e) high-resolution Co 2p XPS spectrum, (f) XPS valence band spectra, (g) TGA and (h, i) N_2 adsorption/desorption isotherm curves for N-CNCS.

polymerization and high temperature carbonization (800 °C) of 3-hydroxytyramine hydrochloride, a high crystalline graphene shell layer can form on the surface of the silica micro-sphere. According to the diameter of N-CNCS nanoparticles, *i.e.*, ~85.84 nm (Fig. 1f), the thickness of the graphene shell layer of N-CNCS nanoparticles was calculated *via* TEM analysis to be about 16 nm. Accordingly, this small size and ordered frameworks can greatly shorten the lithium diffusion length and facilitate the electrochemical reactions, thereby leading to a potentially high electrochemical performance.[26,27]

The crystallinity and chemical composition of the as-obtained N-CNCS nanomaterials were firstly evaluated by the X-ray diffraction (XRD). The obtained pattern in Fig. 2a manifests the typical diffraction peak of N-CNCS located at 44.39°, indexed as (101) planes, which matches that of the crystallized hexagonal system graphene (JCPDS #41-1487). The sharp diffraction peaks suggest the high crystallinity of the graphene shell layer in N-CNCS occurred as a result of high-temperature (800 °C) calcination process. It is worth noting that no discernible diffraction peaks arisen from the residual Co nanoparticles are observed for N-NCS because of their low amount of the composite. Raman spectra are also recorded for N-CNCS and illustrated in Fig. 2b. Noticeably, two remarkable peaks at 1354.47 cm^{-1} and 1594.61 cm^{-1} are attributed to the D band related to disordered carbon, and G band associated with a graphitic structure (sp^2 hybridized carbon), respectively. I_D/I_G ratio values were found to be ~0.869, indicating the high degree of graphitization, which would enhance the electrical conductivity of the nanocomposite.[28] The surface chemical compositions and valence states were further examined by X-ray photoelectron spectroscopy (XPS), as shown in Fig. 2c–f, in which the wide survey XPS profiles of N-CNCS demonstrates the presence of C, N and O elements. The high-resolution spectrum of N 1s in Fig. 2d shows two split peaks at 398.58 eV (pyridinic-N) and 401.76 eV (graphitic-N). The higher content of pyridinic-N, *i.e.*, 85.16%, could further enhance the electronic conductivity of the carbon material.[29] Indeed, no Co 2p peaks were detected for N-CNCS, which is in agreement with the XRD analysis that the Co metal was leached using a strong acid. Besides, Fig. 2f displays the valence band of N-CNCS in 4.62 eV. The thermogravimetric analysis (TGA) conducted in air confirmed the mass fraction of N-CNCS in the composite to be 93.55% (Fig. 2g). The relatively high content of the carbon matrix is expected to allow the nanocomposite to achieve stable and fast-charge storage.[14] The obtained nitrogen sorption isotherms indicate that N-CNCS have a high Brunauer–Emmett–Teller (BET) surface area of 145.67 $m^2\ g^{-1}$ along with an average pore size of 3.5 nm (Fig. 2h and i). The amount of the silica microsphere has a great influence on its BET surface. When the additive amount is 0.2 g and 1.2 g, the BET surface is 111.11 $m^2\ g^{-1}$, and 96.04 $m^2\ g^{-1}$, respectively. This high surface area of N-CNCS combined with its unique macropores features could be beneficial to the electrolyte penetration and fast ion diffusion.[30]

The N-CNCS material was synthesized by adding different amounts of silica micro-spheres and resulted in three samples of nitrogen-doped carbon nanocages. It should be noted that the fine-tuning of the amount of utilized hard template in the hydrothermal treatment plays a key role in the successful synthesis of homodisperse N-CNCS. Fig. 3a shows that the carbon nanocages have a rough and corrugated surface with abundant lamellar structures with 0.2 g silica micro-spheres (aggregated N-CNCS, denoted as A-N-CNCS). With increasing the amount of silica micro-spheres from 0.2 g to 0.7 g (N-CNCS) and then 1.2 g, compared with the corrugated carbon nanocages, a relatively smooth surface can be observed for the hollow carbon spheres (smooth N-CNCS, denoted as S-N-CNCS for 1.2 g silica micro-spheres), and the highly crumpled nitrogen-doped carbon shells turn into the very thin carbon layers (Fig. 3b and

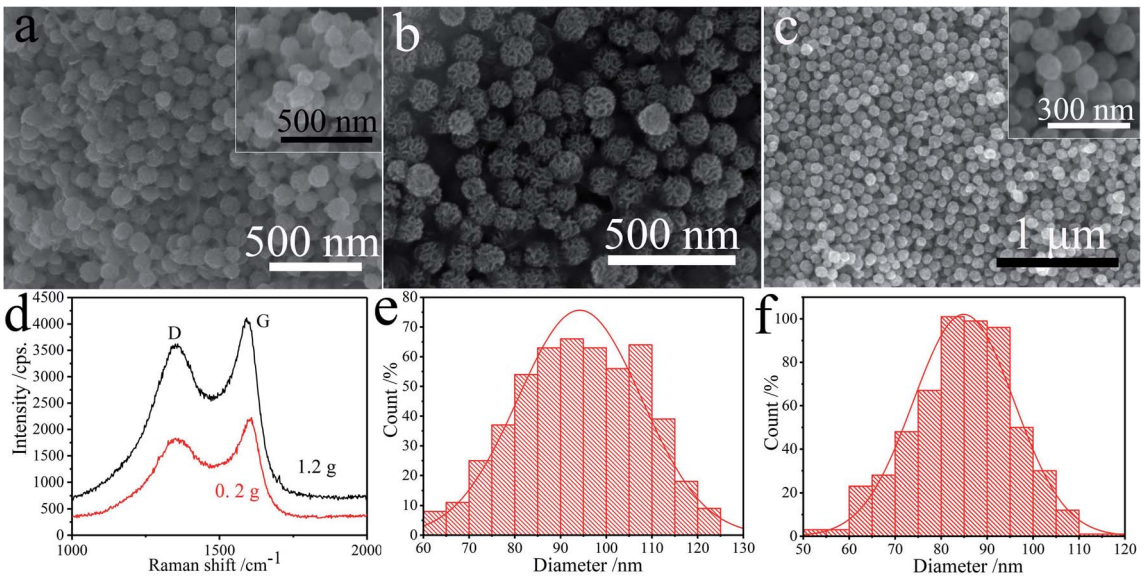

Fig. 3 Typical FESEM images of N-CNCS with adding (a) 0.2 g, (b) 0.7 g and (c) 1.2 g silica micro-spheres. (d) Raman spectra and (e, f) Particle size distribution of A-N-CNCS and S-N-CNCS, respectively.

c). Fig. 3d compares Raman spectra of the two samples, which show a similar D-band and G-band peaks. Noticeably, the intensity ratio of A-N-CNCS is weaker ($I_D/I_G = 0.817$), compared to that of N-CNCS ($I_D/I_G = 0.869$) and S-N-CNCS ($I_D/I_G = 0.883$), indicating that the increased amount of silica micro-spheres introduces more defects and disorder structures into the carbon lattice under a consistent calcination condition.[7] The equivalent average size of A-N-CNCS is statistically measured to be ~94.22 nm, while that of S-N-CNCS is ~83.92 nm (Fig. 3e and f).

3.2 Electrocatalytic performance

The discharge curves of Li/SO_2Cl_2 catalyzed by the acetylene carbon black mixed with N-CNCS in different proportions are shown in Fig. 4a. According to the discharge graph of the pristine electrode using the acetylene carbon black, the initial voltage and discharge time is 3.248 V, and 700 s, respectively. Noticeably, the initial voltage and discharge time were improved when N-CNCS as the electrochemical catalyst was added to the acetylene carbon black electrode. Accordingly, the optimal performance, *i.e.*, the initial voltage of 3.58 V with a discharge time of 840 s, was achieved in a mixed amount of 2.0% with a wider discharge platform and slower voltage drop. The relative capacity and rate capability can be calculated using eqn (1) and (2) (ref. 31) as follow.

$$c = \int I\mathrm{d}t = \int \frac{U}{\mathrm{Re}}\mathrm{d}t = \sum \frac{U}{\mathrm{Re}}\mathrm{d}t = \frac{1}{\mathrm{Re}}\sum U\mathrm{d}t \quad (1)$$

$$X = \frac{C - C_0}{C_0} \times 100\% \quad (2)$$

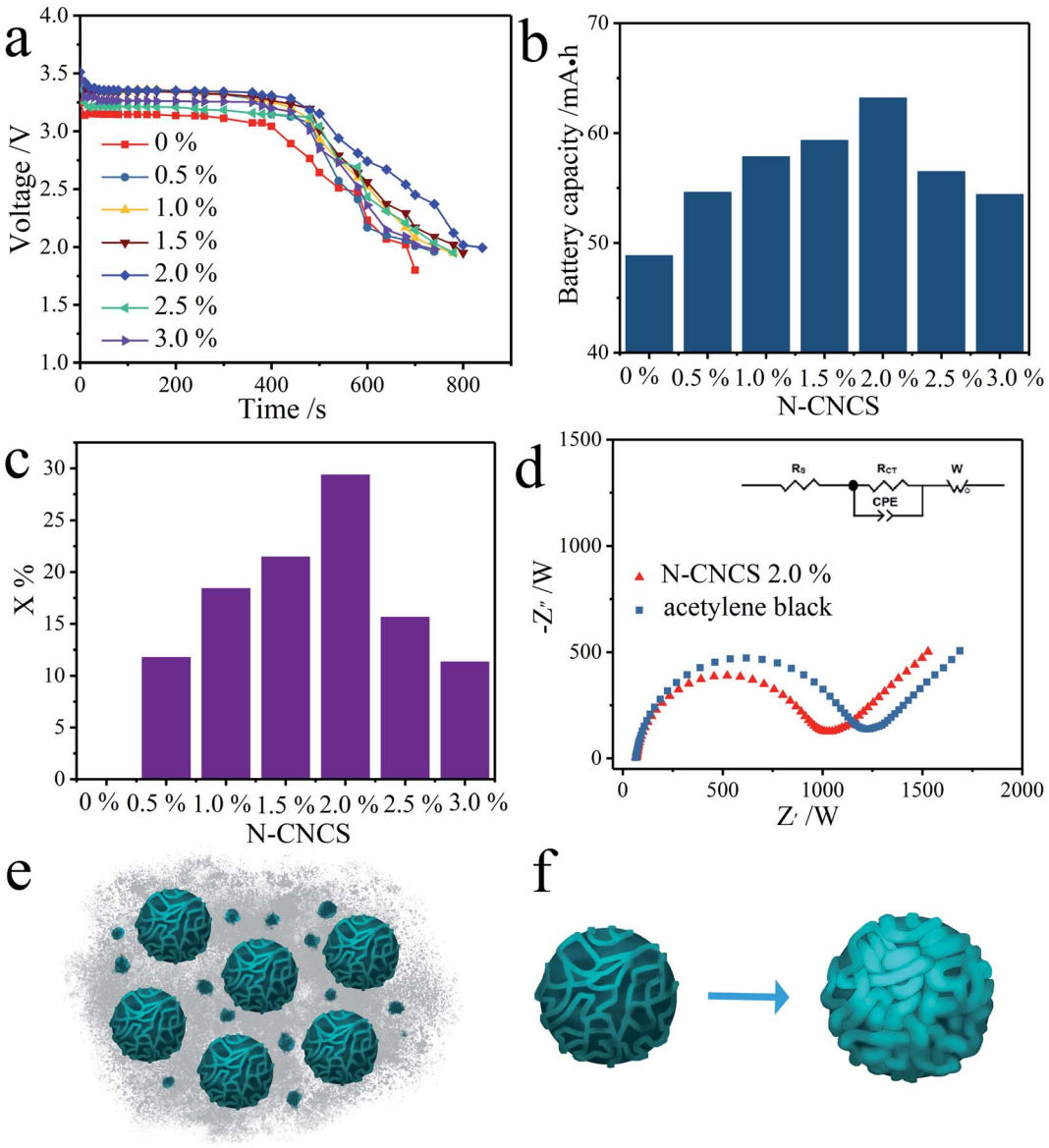

Fig. 4 (a) The discharge curves, (b) capacity and (c) rate capability of Li/SO_2Cl_2 batteries using different proportions of N-CNCS. (d) Electrochemical impedance spectra of acetylene black and N-CNCS (mixed ratio: 2.0%), the inset is the equivalent circuits. (e) Schematic diagram of the mixed electrode (the grey part represents acetylene carbon black). (f) Schematic diagram of N-CNCS in the discharge process.

where C stands for capacity of the battery, C_0 represents the capacity in absence of N-CNCS, I and U are the discharge current and the voltage, respectively, Re is the constant load in the test, about 40 Ω, and Δt stands for the discharging time.

As a result of the electro-catalyzing effect of 2.0% mixed N-CNCS, the relative capacity and rate capability of the Li/SO_2Cl_2 battery were increased to a certain extent (Fig. 4b and c), compared to those of the pristine electrode. Hence, the proper mass ratio between N-CNCS and acetylene carbon black is crucial for the electrochemical properties of the Li/SO_2Cl_2 battery. The excessive amount of N-CNCS may aggravate, leading to a rapid decline of the voltage and capacity.[18,32] The impedance data of the cells with and without N-CNCS is also given (Fig. 4d), it can be concluded that the diameters of the semicircle (Rct) for the N-CNCS electrodes (1010 Ω) is significantly smaller than that of the pure acetylene carbon black electrode (1254 Ω), revealing that the additional N-CNCS is beneficial for reducing the charge resistance by improving the electronic conductivity at the electrode–electrolyte interface. Therefore, the electrode with above-mentioned optimal composition exhibits a superior capacity and discharge performance compared to that with the pristine composition (Fig. 4e), owing to better Li-ion intercalation/deintercalation and ion adsorption/desorption properties come from N-CNCS nanocomposite powder as the active material in the porous and conductive electrode.[3,26] N-CNCS with internal pores and nitrogen-doped graphene shell are highly conductive and stable. They can not only prevent the structural degradation, but also provide ultrafast pathways for ion and electron transport to overcome the slow kinetics of the acetylene black material.[33–35] At the same time, the resultant sediments like LiCl and S can form a film and coat the carbon electrode surface, causing a voltage and capacity decay. As schematically illustrated in Fig. 4f, when Li^+ is intercalated into the lattice of the N-CNCS and while SO_2Cl_2 is adsorbed onto its surface, the caused volume expansion will fill up all space in N-CNCS, and the inner pores can effectively stay interconnected, which can facilitate a rapid ion diffusion through the active materials, and may explain the outstanding electrochemical performance of the N-CNCS.

4. Conclusions

In summary, an electrode material for Li/SO_2Cl_2 batteries made of nitrogen-doped carbon nanocages with high surface roughness was synthesized *via* a simple heating strategy. As revealed by the detailed characterization techniques, such porous graphene nanocages comprise more activated carbon pores, providing shorter pathways and stable structure for fast and safe ion and electron transport. Moreover, a full-cell was assembled to investigate the performance of the N-CNCS, demonstrating a high initial voltage of 3.58 V and a long discharge time of 840 s. The capacity of 63.20 mA h was achieved in the sample with a mixed amount of 2.0% N-CNCS, which is higher than that of the pristine electrode with only acetylene carbon black by a rate of 29.36%. The superior electrochemical performance is primarily attributed to the superior interface properties due to the conductive and porous graphene shell layer along with the N-doping effect. Indeed, the combination of flexible graphene and wrinkled structure assures a reversible change of the electrode thickness, resulting in large adsorption ability of Li^+ and SO_2Cl_2, and excellent structural stability. Moreover, the obtained results suggest that this hydrothermal synthesis strategy may be applicable for further researches about Li/SO_2Cl_2 batteries, and promote the application of other carbon material in porous hosts for energy storage and conversion purposes.

Conflicts of interest

There are no conflicts to declare.

Acknowledgements

This work is supported by the National Natural Science Foundation of China (Grant No. 5171141 and 52072298), the Fund of Science and Technology on Electromechanical Dynamic Control Laboratory (No. 9140C3608061002).

References

1 R. M. Spotnitz, G. S. Yeduvaka, G. Nagasubramanian and R. Jungst, Modeling self-discharge of Li/SOCl2 cells, *J. Power Sources*, 2006, **163**, 578–583.
2 M. S. Guney and Y. Tepe, Classification and assessment of energy storage systems, *Renewable Sustainable Energy Rev.*, 2017, **75**, 1187–1197.
3 J. Berger, G. Laske, J. Babcock and J. Orcutt, An ocean bottom seismic observatory with near real-time telemetry, *Earth and Space Science: Oceans*, 2016, **3**, 68–77.
4 Y. S. Guo, H. H. Ge, G. D. Zhou and Y. P. Wu, Comparative study on carbon cathodes with and without cobalt phthalocyanine in Li/($SOCl_2$ + BrCl) cells, *J. Power Sources*, 2009, **194**, 508–514.
5 M. Ue and K. Uosaki, Recent progress in liquid electrolytes for lithium metal batteries, *Curr. Opin. Electrochem.*, 2019, **17**, 106–113.
6 Y. Zhang, *et al.*, Improving electrocatalytic activity of fluorinated multi-walled carbon nanotubes modified with tetraaminophthalocyanines for lithium/thionyl chloride battery, *Ionics*, 2019, **25**, 1459–1469.
7 M. Tian, R. Li, C. Liu, D. Long and G. Cao, Aqueous Al-Ion Supercapacitor with V_2O_5 Mesoporous Carbon Electrodes, *ACS Appl. Mater. Interfaces*, 2019, **11**, 15573–15580.
8 C. Zhan, X. Zeng, X. Ren, Y. Shen, R. Lv, F. Kang and Z. Huang, Dual-ion hybrid supercapacitor: Integration of Li-ion hybrid supercapacitor and dual-ion battery realized by porous graphitic carbon, *J. Energy Chem.*, 2020, **42**, 180–184.
9 D. Zhang, S. Wang, B. Li, Y. Gong and S. Yang, Horizontal Growth of Lithium on Parallelly Aligned MXene Layers towards Dendrite-Free Metallic Lithium Anodes, *Adv. Mater.*, 2019, **31**, 6–11.
10 Z. Xiao, Z. Li, P. Li, X. Meng and R. Wang, Ultrafine Ti_3C_2 MXene Nanodots-Interspersed Nanosheet for High-Energy-

Density Lithium-Sulfur Batteries, *ACS Nano*, 2019, **13**, 3608–3617.

11 Y. Yu, Z. Guo, Q. Peng, J. Zhou and Z. Sun, Novel two-dimensional molybdenum carbides as high capacity anodes for lithium/sodium-ion batteries, *J. Mater. Chem. A*, 2019, **7**, 12145–12153.

12 Q. Yun, L. Li, Z. Hu, Q. Lu, B. Chen and H. Zhang, Layered Transition Metal Dichalcogenide-Based Nanomaterials for Electrochemical Energy Storage, *Adv. Mater.*, 2020, **32**, 1–29.

13 J. Duan, *et al.*, Lithium–Graphite Paste: An Interface Compatible Anode for Solid-State Batteries, *Adv. Mater.*, 2019, **31**, 1–7.

14 W. Fu, E. Zhou, R. Ma, Z. Sun, Y. Yang, M. Sevilla, A. B. Fuertes, A. Magasinski and G. Yushin, Anatase TiO_2 Confined in Carbon Nanopores for High-Energy Li-Ion Hybrid Supercapacitors Operating at High Rates and Subzero Temperatures, *Adv. Energy Mater.*, 2020, **10**, 1902993.

15 K. Chen, *et al.*, Metal–Organic Frameworks (MOFs)-Derived Nitrogen-Doped Porous Carbon Anchored on Graphene with Multifunctional Effects for Lithium–Sulfur Batteries, *Adv. Funct. Mater.*, 2018, **28**, 1–8.

16 J. B. Cook, *et al.*, Pseudocapacitive Charge Storage in Thick Composite MoS_2 Nanocrystal-Based Electrodes, *Adv. Energy Mater.*, 2017, **7**.

17 A. Muzaffar, M. B. Ahamed, K. Deshmukh and J. Thirumalai, A review on recent advances in hybrid supercapacitors: Design, fabrication and applications, *Renewable Sustainable Energy Rev.*, 2019, **101**, 123–145.

18 C. Yang, *et al.*, $ZnFe_2O_4$ @ Carbon Core – Shell Nanoparticles Encapsulated in Reduced Graphene Oxide for High-Performance Li-Ion Hybrid Supercapacitors, *ACS Appl. Mater. Interfaces*, 2019, **11**, 14713–14721.

19 F. Béguin, V. Presser, A. Balducci and E. Frackowiak, Carbons and electrolytes for advanced supercapacitors, *Adv. Mater.*, 2014, **26**, 2219–2251.

20 X. Liu, *et al.*, A MoS_2/Carbon hybrid anode for high-performance Li-ion batteries at low temperature, *Nano Energy*, 2020, **70**, 104550.

21 G. Wang, *et al.*, Stabilization of Sn Anode through Structural Reconstruction of a Cu–Sn Intermetallic Coating Layer, *Adv. Mater.*, 2020, **32**, 1–9.

22 Z. Wu, *et al.*, Highly Conductive Two-Dimensional Metal-Organic Frameworks for Resilient Lithium Storage with Superb Rate Capability, *ACS Nano*, 2020, **14**, 12016–12026.

23 B. Jiang, C. Han, B. Li, Y. He and Z. Lin, In-Situ Crafting of $ZnFe_2O_4$ Nanoparticles Impregnated within Continuous Carbon Network as Advanced Anode Materials, *ACS Nano*, 2016, **10**, 2728–2735.

24 T. X. Nguyen, J. Patra, J. K. Chang and J. M. Ting, High entropy spinel oxide nanoparticles for superior lithiation-delithiation performance, *J. Mater. Chem. A*, 2020, **8**, 18963–18973.

25 S. Huang, *et al.*, Free-standing 3D composite of CoO nanocrystals anchored on carbon nanotubes as high-power anodes in Li-Ion hybrid supercapacitors, *J. Power Sources*, 2019, **437**, 226934.

26 J. Zhang, *et al.*, High Intercalation Pseudocapacitance of Free-Standing T-Nb_2O_5 Nanowires@carbon Cloth Hybrid Supercapacitor Electrodes, *J. Electrochem. Soc.*, 2017, **164**, A820–A825.

27 V. Augustyn, *et al.*, High-rate electrochemical energy storage through Li^+ intercalation pseudocapacitance, *Nat. Mater.*, 2013, **12**, 518–522.

28 J. Xie, J. Ye, F. Pan, X. Sun, K. Ni, H. Yuan, X. Wang, N. Shu, C. Chen and Y. Zhu, Incorporating Flexibility into Stiffness: Self-Grown Carbon Nanotubes in Melamine Sponges Enable A Lithium-Metal- Anode Capacity of 15 $mAhcm^{-2}$ Cyclable at 15 $mAcm^{-2}$, *Adv. Mater.*, 2019, **31**, 1805654.

29 W. Yuan, *et al.*, A flexible 3D nitrogen-doped carbon foam @ CNTs hybrid hosting TiO_2 nanoparticles as free-standing electrode for ultra-long cycling lithium-ion batteries, *J. Power Sources*, 2018, **379**, 10–19.

30 J. H. Park, *et al.*, Etching-Assisted Crumpled Graphene Wrapped Spiky Iron Oxide Particles for High-Performance Li-Ion Hybrid Supercapacitor, *Small*, 2018, **14**, 1704209.

31 Y. Gao, *et al.*, A series of new Phthalocyanine derivatives with large conjugated system as catalysts for the Li/$SOCl_2$ battery, *J. Electroanal. Chem.*, 2018, **808**, 8–13.

32 S. Zhang, *et al.*, High Performance Lithium-Ion Hybrid Capacitors Employing Fe_3O_4-Graphene Composite Anode and Activated Carbon Cathode, *ACS Appl. Mater. Interfaces*, 2017, **9**, 17136–17144.

33 T. Chen, *et al.*, High performance binder-free SiOx/C composite LIB electrode made of SiOx and lignin, *J. Power Sources*, 2017, **362**, 236–242.

34 A. Muzaffar, M. B. Ahamed, K. Deshmukh and J. Thirumalai, A review on recent advances in hybrid supercapacitors: Design, fabrication and applications, *Renewable Sustainable Energy Rev.*, 2019, **101**, 123–145.

35 K. Li, *et al.*, Cobalt tetrapyridinoporphyrazine nanoparticulates anchored on carbon nanotubes for long-voltage Li/$SOCl_2$ batteries, *Electrochim. Acta*, 2019, **295**, 569–576.